Accepted Article Preview: Published ahead of advance online publication

In-situ real-time monitoring of ultrafast laser processing using wide-field high-resolution snapshot compressive Microscopy

Xiaodong Wang, Miao Cao, Ziyang Chen, Jiao Geng, Ting Luo, Yufei Dou, Xing Liu, Liping Shi, and Xin Yuan

Cite this article as: Xiaodong Wang, Miao Cao, Ziyang Chen, Jiao Geng, Ting Luo, Yufei Dou, Xing Liu, Liping Shi, and Xin Yuan. In-situ real-time monitoring of ultrafast laser processing using wide-field high-resolution snapshot compressive Microscopy. *Light: Advanced Manufacturing* accepted article preview 17 May, 2024; doi: 10.37188/lam.2024.029

Received 02 November 2023; revised 13 May 2024; accepted 14 May 2024; Accepted article preview online 17 May 2024

In-situ real-time monitoring of ultrafast laser processing using wide-field high-resolution snapshot compressive microscopy

Xiaodong Wang[1 2], Miao Cao[1 2], Ziyang Chen[4], Jiao Geng[3], Ting Luo[2], Yufei Dou[2], Xing Liu[2], Liping Shi[3 *], and Xin Yuan[2 5 6 *]

[1]*Zhejiang University, Hangzhou 310027, China*
[2]*Research Center for Industries of the Future and School of Engineering, Westlake University, Hangzhou 310030, China*
[3]*Hangzhou Institute of Technology, Xidian University, Hangzhou 311231, China*
[4]*School of Physics, Harbin Institute of Technology, Harbin 150001, China*
[5]*Westlake Institute for Optoelectronics, Fuyang, Hangzhou 311421, China*
[6]*Key Laboratory of 3D Micro/Nano Fabrication and Characterization of Zhejiang Province, Westlake University, 310024 Hangzhou, China*
*Correspondence to: Liping Shi: shiliping@xidian.edu.cn or Xin Yuan: xyuan@westlake.edu.cn

Abstract

Over the last decades, ultrafast laser processing has become a widely used tool for manufacturing of micro- and nanostructure. Real time monitoring of laser material processing opens opportunities to inspect the process and provide feedback. To date, *in-situ* and real-time monitoring of laser material processing is rarely performed. Towards this end, in this paper, we propose a dual-path snapshot compressive microscopy (DP-SCM) for high-speed, large field-of-view and high-resolution imaging for *in-situ* and real-time ultrafast laser processing. In the evaluation of DP-SCM, the field-of-view, lateral resolution and imaging speed are measured to be 2 mm, 775 nm and 500 fps respectively. In ultrafast laser processing, the laser scanning process is observed by DP-SCM system when translating the sample stage and scanning the focused femtosecond laser respectively. Finally, we have monitored the development of self-organized nano-gratings structure, validating our system's potential to unveil new material mechanisms. The proposed method serves as an add-up (plug-and-play) module to any imaging setup and has vast potential in opening up new avenues for high-throughput imaging in laser material processing.
Keywords: Snapshot compressive imaging, Femtosecond laser processing, Laser-induced self-organization

Introduction

Processing of materials by ultrafast pulsed laser has opened opportunities in modern microfabrication and production. The advancement in generating ultrashort laser pulses, spanning from femtoseconds (fs) to a few picoseconds (ps) in duration, has facilitated the commercial availability of ultrafast laser systems at a reasonable cost. As a result, this development has empowered numerous researchers to conduct comprehensive investigations into interactions between light and matter under extremely high irradiance conditions [1, 2, 3, 4, 5, 6, 7, 8]. For example, in transparent substrate, the interaction with short, intense laser pulses can lead to nonlinear absorption phenomena, such as 'multiphoton' absorption [9], during which the laser radiation is locally absorbed. In the case of fused silica, a localised increase of density may appear, which is useful for inscribing direct-write waveguide [10, 11] and triggering self-organised nanostructures [12, 13, 14, 15].

The quality of components produced through ultrafast laser manufacturing is greatly affected by the production process parameters. For example, the typical threshold for generating strong thermal accumulation may depend

on parameters like the laser pulse energy, pulse duration, scan speed, and material properties. Extensive tuning of the laser-parameter is thereby required for a single material. As a result, sensors and measurement systems are readily accessible for monitoring the energy source and materials. Commonly used techniques include X-ray tomography [16], laser scanning confocal microscopy [17], scanning electron microscopy [18] and optical coherence tomography [19]. However, most of these approaches are carried out in an *ex-situ* manner, that is, an iterative optimization of a set of parameters is performed on the finished structures. Such operation requires time-consuming analysis and significant production cost.

In general, *in-situ* and real-time monitoring of ultrafast laser material processing is of great importance to the manufacturing field. There are several instances of this in the literature [20, 21, 22, 23]. An *in-situ* monitoring method commonly used in the context of ultrafast laser manufacturing is wide-field optical microscopy [20]. This approach involves capturing two-dimensional snapshots of light scattering, revealing the transient refractive-index distribution arising from different sample regions. Another *in-situ* method is optical coherence tomography [21, 22], which allows for assessing the quality and properties of 3D microstructures in real-time scenario. Apart from the above methods, broadband coherent anti-Stokes Raman scattering (CARS) microscopy is shown to be an *in-situ* and real-time tool for observing the microscopic characterization of structures fabricated by two-photon polymerization [23]. However, these microscopic approaches are comparatively slow in imaging speed. This limitation arises from the fact that imaging speed is primarily determined by camera frame rate and data bandwidth. In certain dynamic scenarios where the laser-material interaction happens at much higher speed (over 500fps), high-speed imaging and big data storage are of paramount importance. Furthermore, considering spatial bandwidth, achieving a comprehensive and detailed analysis requires an innovative optical configuration characterized by a wide field-of-view (FOV) and high resolution. In general, high-throughput data does not meet the demands for real-time imaging. Hence conventional microscopic imaging is not suitable for routine on-the-fly in-process monitoring.

An optimal *in-situ* and real-time imaging method should meet four key criteria: large FOV, high resolution, fast imaging speed and low data bandwidth. However, traditional microscopy techniques have limited functionality when it comes to capturing high-resolution images of large areas quickly. There are several ways to increase FOV and resolution simultaneously. Direct ways involve using objective lens with high numerical aperture or increasing sensor size [24, 25]. Both methods require expensive hardware, leading to increased costs. Another approach is using computational techniques such as Fourier Ptychography [26, 27]. This method involves acquiring a series of low-resolution images and computationally merging them to produce a high-resolution image. This process is time-consuming and fails to reconstruct high-speed scenes. Instead of employing the methods mentioned above, we opt for a straightforward bipath approach to distinguish between the high-resolution and wide FOV paths. This approach consists of two parallel optical paths: one is optimized for high-resolution imaging, while the other is designed for wide-field imaging.

A promising approach for addressing the limited imaging speed and data storage is snapshot compressive imaging [28, 29, 30, 31, 32, 33, 34, 35, 36, 37, 38], which combines hardware encoder and software decoder to enable high-speed imaging in a snapshot. This technique uses temporally varying masks to modulate scenes and a regular CCD/CMOS camera for detection. Compressed ultrafast photography (CUP) follows a similar principle to snapshot compressive imaging but distinguishes itself by employing temporally sheared masks for modulation and a streak camera for scene capture [39, 40, 41, 42, 43, 44, 45]. Leveraging the streak camera's ultrafast electronic response, CUP stands out as the world's fastest camera, capable of capturing transient dynamic events at a staggering speed of 100 billion frames per second. This breakthrough has enabled applications such as measuring the speed of light [39] and fluorescence lifetime imaging [41]. However, the streak camera is significantly costlier, approximately 100 times more expensive than CCD/CMOS alternatives. This substantial price difference restricts its practical use among ordinary researchers. Employing a chirped pulse for illumination can eliminate the necessity of a streak camera to capture ultrafast processes [45]. Nevertheless, it is challenging to image self-illuminating processes such as fluorescence processes. Hence, in this paper we turn to a more practical and low-cost solution – snapshot compressive imaging. By harnessing advanced deep learning reconstruction algorithms [32, 33, 34, 36, 35, 37, 38], we can decode the high-speed scene from a snapshot measurement, hence lowing the data storage while increasing the imaging speed simultaneously.

In this paper, we demonstrated, for the first time, *in-situ* and real-time monitoring of ultrafast laser material processing using snapshot compressive microscopy. Specifically, to mitigate the inherent trade-off between spatial resolution, FOV and imaging speed, we propose a dual-path snapshot compressive microscopy (DP-SCM) for laser material processing. DP-SCM consists of two parallel optical paths, one optimized for high-resolution imaging and the other for wide-field imaging. By combining these dual measurements, DP-SCM can reconstruct high-resolution images over a large FOV at high imaging speed. In the Principle section, we describe the fundamental principle and derive the mathematical formulation of snapshot compressive imaging. In the Results and Discussion section,

the experimental setup was shown. We then validated its capability in terms of FOV, lateral resolution, imaging speed and reconstruction algorithm using a high-resolution target. Furthermore, to verify the feasibility of DP-SCM for *in-situ* and real-time monitoring in femtosecond laser processing, we observed the laser scanning process when translating the sample stage and rotating the scanning mirror respectively. Lastly, we investigated the growth of self-organized periodic structure using our DP-SCM system. When a high-speed camera is running at 1000fps, we have closely monitored the development of nano-gratings, validating our system's potential to unveil new material mechanisms due to its discoveries.

Principle

Fig. 1 depicts the sensing process of snapshot compressive imaging, which can be divided into optical encoding, compressive measurement and reconstruction. The high-speed dynamic scene, modelled as a time-series of two-dimensional images, is firstly collected by the objective lens and relayed to the digital micromirror device (DMD) or shifting mask, known as the optical encoder. The optical encoder imposes spatially-varying binary mask at each timestamp to encode the high-speed scenes. The modulated scene is then relayed onto the camera. To capture the dynamic scenes in a single shot of the camera, multiple variant masks are displayed on the optical encoder within the camera exposure. A snapshot on the camera integrates tens of temporal frames of the high-speed scene, forming a compressive measurement. Lastly, by feeding the compressive measurement and pre-measured masks into the iterative algorithms or deep neural networks, the high-speed scene can be well reconstructed.

We now formulate the forward imaging model of snapshot temporal compressive imaging system. Let (x, y, t) denotes the spatial-temporal coordinate system of a dynamic scene $\mathbf{O}(x, y, t)$. We define the temporal varying masks to be represented as $\mathbf{C}(x, y, t)$. The compressed measurement is modelled as the temporal integration of the product between the corresponding masks and scene,

$$I(x', y') = \int_{t=0}^{T} O(x, y, t) \bullet C(x, y, t) dt \tag{1}$$

where $I(x', y')$ is the continuous representation of the compressed measurement over an exposure time T.

In discretized form, considering B discrete time slots, B high-speed frames $\{\mathbf{X}_k\}_{k=1}^{B} \in \mathbb{R}^{n_x \times n_y}$ are modulated by the coding masks $\{\mathbf{M}_k\}_{k=1}^{B} \in \mathbb{R}^{n_x \times n_y}$. The discretized measurement is thus given by,

$$\mathbf{Y} = \sum_{k=1}^{B} \mathbf{X}_k \odot \mathbf{M}_k + \mathbf{G} \tag{2}$$

where $\odot$ denotes the element-wise product. $\mathbf{G} \in \mathbb{R}^{n_x \times n_y}$ represents the measurement noise. We then vectorize the sensing process. Define

$$\mathbf{x} = \left[\mathbf{x}_1^{\mathbf{T}}, ..., \mathbf{x}_B^{\mathbf{T}}\right]^{\mathbf{T}} \tag{3}$$

where $\mathbf{x}_k = \mathbf{vec}(X_k)$ represents the vectorized formulation of the k-th frame by stacking the columns. Let

$$\Phi = [\mathbf{D}_1, ..., \mathbf{D}_B] \tag{4}$$

where $\mathbf{D}_k = Diag(\mathbf{vec}(\mathbf{M}_k))$ represents the diagonal formulation of $\mathbf{M}_k$ of the k-th frame, where each diagonal element corresponds to the value in its vectorized form. By reshaping the Eq. (2) using $\mathbf{x}$ and Φ, we obtain the sensing process in its vectorized formulation,

$$\mathbf{y} = \mathbf{\Phi x} + \mathbf{g} \tag{5}$$

where $\mathbf{y} = \mathbf{vec}(\mathbf{Y})$ and $\mathbf{g} = \mathbf{vec}(\mathbf{G})$. This formulation resembles the concept of compressed sensing, but it involves a unique structure in the sensing matrix Φ. We aim to recover $\mathbf{x}$ given the measurement $\mathbf{y}$ and mask Φ. This is a typical ill-posed inverse problem, which can be solved by the optimization-based or deep-learning based methods. In the optimization-based methods, an additional term $\mathbf{R}(\mathbf{x})$ is introduced as a regularization term, which serves as prior information used to constrain the solution. To be more specific, we can represent the reconstruction process as the following optimization task,

$$\hat{\mathbf{x}} = \arg\min_{\mathbf{x}} ||\mathbf{y} - \mathbf{\Phi x}||_2^2 + \tau \mathbf{R}(\mathbf{x}) \tag{6}$$

where τ is a parameter to balance the data fidelity term $||\mathbf{y} - \mathbf{\Phi x}||_2^2$ and the regularization term $\mathbf{R}(\mathbf{x})$. To solve the ill-posed problem, various iterative algorithms have been proposed [35, 36]. Another solution to Eq. (5) is to learn the inverse modeling between the measurement $\mathbf{y}$ and the desired signal $\mathbf{x}$ through deep neural network [32, 33, 34, 37]. Formally, deep-learning based algorithm minimizes the following problem through gradient descent (such as Adam optimizer [46]),

$$\hat{\mathbf{w}} = \arg\min_{\mathbf{w}} ||\mathbf{y} - \mathbf{\Phi}(\mathbf{N}(\mathbf{w}))||_2^2 \tag{7}$$

where $\mathbf{w}$ is the learnable weight, which is optimized through training. After training, the reconstructed signal $\hat{\mathbf{x}}$ can be obtained instantly by feeding the measurement $\mathbf{y}$ into the pre-trained neural network.

Results and Discussion

Experimental setup

The scheme of our custom-built snapshot compressive microscope is shown in Fig. 2. The setup is mainly composed of a femtosecond laser processing system, a high-resolution snapshot compressive microscope and a wide field-of-view snapshot compressive microscope. The femtosecond laser (Fs laser, FLASH-100-IR, ULTRON

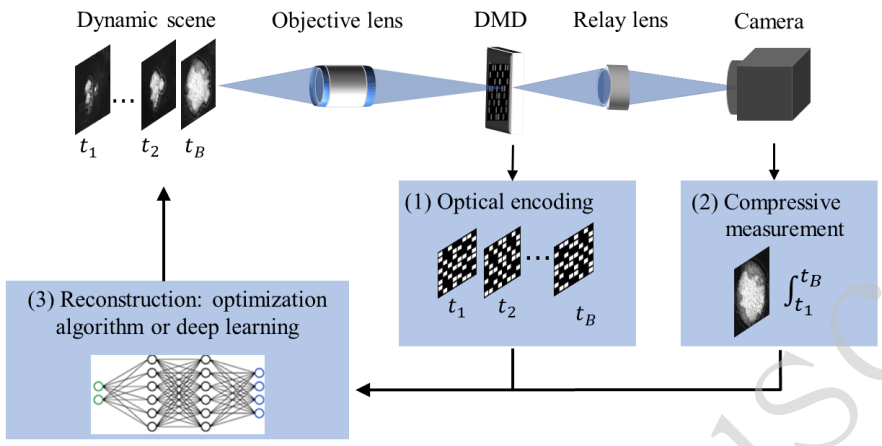

Fig. 1. Principle of snapshot compressive imaging, which consists of optical encoding, compressive measurement and reconstruction.

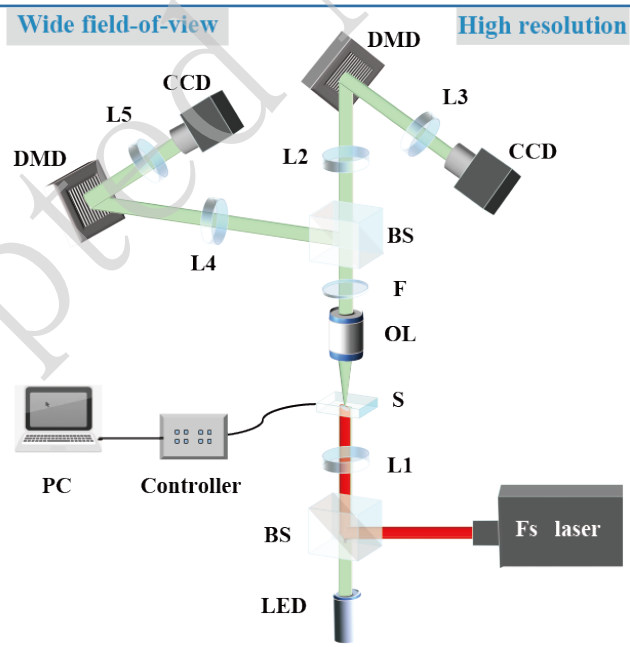

Fig. 2. Experimental setup of DP-SCM system: L1-L5, lens; OL, objective lens; BS, beamspliter; Fs laser: femtosecond laser; S: sample. F: IR cut filter. DMD: digital micromirror device. LED: light-emitting diode.

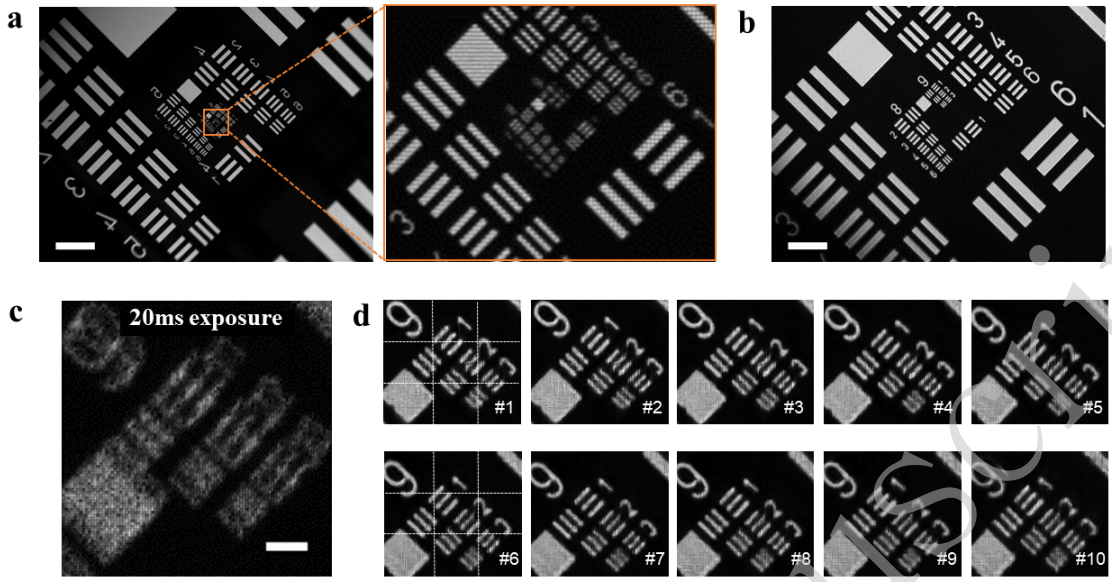

Fig. 3. Performance evaluation of DP-SCM system. **a** Wide field-of-view image (left) captured by FOV path, with zoom-in image (right). **b** High resolution image captured by the HR path. **c** Compressed measurement under an exposure time of 20ms, compressed ratio of 10. **d** Reconstructed frames from compressed measurement in **c**. Scale bars in **a**, **b** and **c** are 500um, 50um and 5um respectively.

Photonics) has a center wavelength of 1030 nm, a pulse duration of 150 fs, a maximum single pulse energy of 0.2 mJ, and a maximum repetition frequency (single pulse) of 10 MHz. The femtosecond laser is radiated and focused to the sample plane through a beamsplitter and lens (L1, f=200 mm). An infrared (IR) cut filter (F) is used after the objective lens to block the processing light. For in-process monitoring of the laser material processing, we employ a dual-path snapshot compressive microscopy system, dubbed DP-SCM. The DP-SCM system consists of two parallel optical paths, each optimized for a different range of lateral resolution and FOV. Taking the high-resolution optical path as an example, a white-light-emitting diode (LED) is used to illuminate the sample in a transmissive and wide-field manner. The sample is attached to a 2-axis motorized translation stage (GCD-202100M, Daheng Optics). The transmissive light from the sample is collected by an objective lens with high numerical aperture (OL, 20×, NA=0.42) and relayed to the digital micromirror (DMD, Vialux, DLP7000, 768×1024 pixel count, 13.7 μm pixel pitch) through a long-focal-length lens (L2, f=400mm). The DMD imposes binary spatial modulation to the scene upon transmission. The modulated scene is then relayed onto the CMOS camera (STC-MBS202POE, Santech, 1624×1240 pixel count, 4.5μm pixel pitch) through another lens (L3, f=100mm). The magnification rate between DMD and camera is 0.66, yielding a 1:2 pixel mapping. The camera maintains a constant frame rate of 50 fps, while the DMD operates at varying frame rates, ranging from 500 to 1000. This leads to compression ratios (CR) spanning from 10 to 20. This corresponds to 10 to 20 times faster imaging speed (To clarify, a CR of 10 represents 10×compression, and so on and so forth). The total magnification of high-resolution path is 26×, which in our case guarantees a high resolution inspection of the sample with limited FOV (about 215 μm). On the wide FOV path, we share the same OL for collection of sample light but choose a small-focal-length lens (L4, f=50 mm) to guarantee a smaller magnification (2.75×). In this way, optical resolution is sacrificed in an exchange of a large FOV (about 2 mm). Note that DMD and CMOS in both paths are identical. Since both paths have their individual FOVs and resolutions, hereafter, we refer to the FOV and HR as the FOV of wide field-of-view path and resolution of high-resolution path respectively in our system.

We begin by validating our setup on USAF resolution target (USAF 1951 Hi-Resolution Target, Edmund), as depicted in Fig. 3. In Fig. 3a-b, a standard USAF1951 test target is used to characterise the FOV and lateral resolution of our DP-SCM system. As shown in Fig. 3a, the full FOV of the system is 2 mm through calculation. However, when zooming into the smaller area, details of the resolution target is totally lost. By employing another high-resolution path, the elements of the ninth group can still be resolved. As shown in Fig. 3b, the lowest element corresponding to a

line spacing of 645 lp/mm (775 nm in linewidth, which is quite close to the theoretical resolution with NA=0.41) is clearly seen in high resolution path compared to the zoom-in image in wide-field path in Fig. 3a. The detailed resolution comparison are presented in Supplement Material Fig. S1.

In addition, we characterize the high speed imaging of DP-SCM system. Fig. 3c-d shows a moving scene of resolution target imaged by our system (see Visualizations 1 for the complete video). Fig. 3c is the compressed measurement captured with an exposure time of 20 ms. Within the exposure time, 10 random masks are displayed on the DMD sequentially, which gives a temporal resolution of 2 ms. By feeding the 10 masks (captured in advance) and compressed measurement into EfficientSCI reconstruction algorithm [34], we manage to reconstruct high-speed scenes corresponding to a frame rate of 500 fps from a compressed measurement captured with a frame rate of 50 fps, as presented in Fig. 3d. It can be seen that the resolution target is moving in a diagonal direction and the elements of the ninth group can still be resolved with sharp edges. Note that all the reconstruction algorithm is conducted in a computer with an NVIDIA A40 GPU.

Next, we compare the reconstruction performance using three algorithms (GAP-TV [36], PnP-FastDVDnet [35] and EfficientSCI [34]), as shown in Fig. 4. For better comparison, we select the first recovered frame from compressed measurement (Fig. 3c) as the baseline. GAP-TV is a regularization-based optimization algorithm to solve the ill-posed problem in Eq. (6). PnP-FastDVDnet is an plug-and-play optimization algorithm, which replaces the denoising step in a typical optimization-based algorithm with a deep denoiser (pre-trained neural network), and leads to better reconstruction and flexibility. Both regularization-based and plug-and-play optimization algorithm have been used in different snapshot compressive imaging systems. We compare both algorithms with state-of-the-art EfficientSCI algorithm (one solution in Eq. (7)) which trains the deep neural network in an end-to-end manner and then inferences efficiently. Specifically, building upon the remarkable achievements of convolution and Transformer in computer vision, we have designed a reconstruction network that leverages the strengths of both techniques. A comparison of the reconstructed resolution target in Fig. 4b reveals the EfficientSCI network's ability to recover more distinct structural details. Regarding the reconstruction time, EfficientSCI achieves a significantly faster interference time of approximately 2.5 seconds for reconstructing a compressed measurement (with a compression ratio of 10 and an image size of 800x800 pixels). This is notably swifter compared to GAP-TV (193 secons) and PnP-FastDVDnet (80 seconds). In practical deployment, EfficientSCI achieves an interference time of approximately 0.9 second when the image size is reduced to 256x256 pixels, which meets the real-time imaging requirement. Hereafter we use EfficientSCI network to reconstruct the dynamic scenes in laser material processing.

Inspection of laser material processing

In-situ real-time monitoring of laser material processing is demonstrated in Fig. 5. We consider using a **Si – TiN** bilayer film on a $\mathbf{Al_2O_3}$ substrate as the processing sample (Fig. 5a). The sample is placed on top of a motorized stage. While in the process of translating the stage, the focused femtosecond laser under intense ultrafast laser irradiation is ablating the material, as shown in Fig. 5b. The repetition rate and laser power in our experiment is 100kHz and 0.5mw respectively. We then use our system to capture the real-time ablating process with the camera working at a frame rate of 50 fps. Fig. 5c and Fig. 5d represent the simultaneously captured measurements by FOV and HR path respectively. Given by respective masks (setting compressed ratio is 10), high-speed laser material processing with 500fps is observed clearly. As illustrated in Fig. 5e and Fig. 5f, there are two paths corresponding to HR and FOV imaging module. This indicates that even a slight movement in the FOV path becomes more pronounced in the HR path. Consequently, the movement in Fig. 5e may be difficult to discern, but it becomes more apparent when magnified in Fig. 5f. The sample stage is moving toward upper-right direction. The dynamic laser material processing can be found in Visualizations 2.

Next, we examine the real-time processing when femtosecond laser is scanning upon the material (Fig. 6b). Upon the same laser parameters and camera setting, we manually scan the mirror while capturing the compressed scenes in the HR path. The measurement and reconstruction are shown in Fig. 6a and Fig. 6c respectively, see Visualizations 3 for the complete video. The femtosecond laser is ablating the material with 10 times higher speed, as compared with the measurement, which is captured at the normal camera frame rate. The scanning occurs in the upper-left direction. Apart from simple scanning of sample stage or steering mirror, our approach extends to monitoring the laser printing process, enabling intriguing applications such as customized pattern creation through laser printing. The experimental result is shown in Supplement Material Fig. S2. We have demonstrated our DP-SCM's feasibility in real-time monitoring of laser material manufacturing, whatever in laser scanning or stage scanning.

Inspection of self-organized periodic nanostructure

To demonstrate DP-SCM's capability in discovering more in-depth laser-material interaction, we investigate inspecting the generation of self-organized nanostrutures. As reported in [13], laser-induced self-organization of periodic nanostructures on highly absorbing materials is commonly attributed to the interference between the laser and surface plasmon polaritons (SPPs), which are initially excited by the surface's inherent roughness. Interference between a laser beam and the prominent surface-scattered

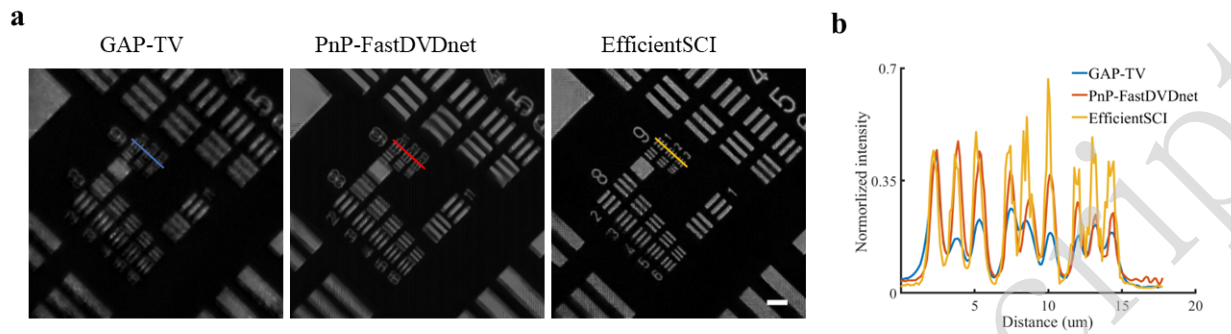

Fig. 4. Comparison of different reconstruction algorithms. **a** Results of GAP-TV, PnP-FastDVDnet, and EfficientSCI. **b** Line profile draw from **a**. Scale bar in **a** is 10um.

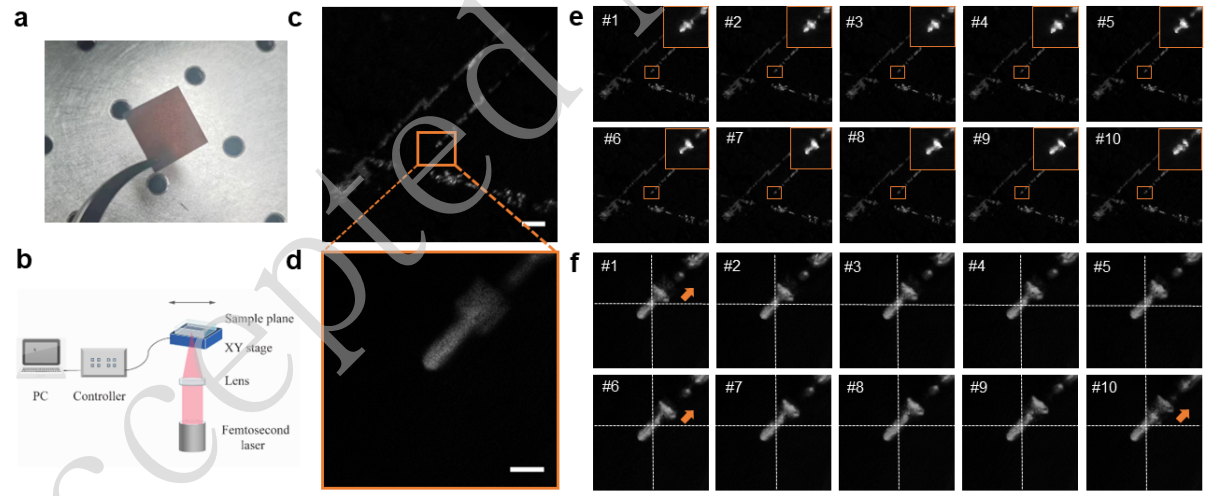

Fig. 5. *In-situ* and real-time monitoring of laser material processing when translating the sample stage. **a** Snapshot of processing material. **b** The translation stage is moving in one direction. **c** Compressed measurement captured by FOV path (exposure time = 20ms, CR=10). **d** Compressed measurement captured by HR path (exposure time = 20ms, CR=10). **e** Reconstruction by EfficientSCI from FOV measurement. **f** Reconstruction by EfficientSCI from HR measurement. Scale bars in **c** and **d** are 200um and 20um respectively.

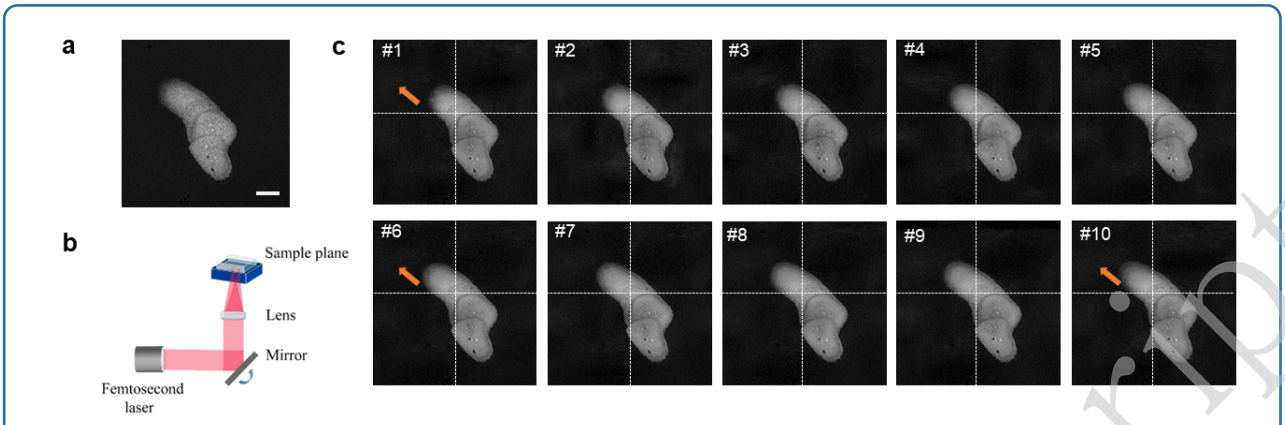

Fig. 6. *In-situ* and real-time monitoring of laser scanning process when scanning the focal point via rotating the mirror. **a** Compressed measurement captured under 20ms in high-resolution path. **b** Schematic of laser scanning process. **c** Reconstructed frames with compressed ratio of 10. Scale bar in **a** is 10um.

waves leads to periodic variations in optical intensity, consequently causing selective modulation of the surface. As a result, periodic nanostructures acquire their long-range alignment and orientation directly influenced by the phase and direction of the surface-scattered waves, with their wavelength determining the structural periodicity. However, these periodic nanostructures often suffer from a lack of consistent regularity.

We first use our DP-SCM system to observe the self-organized periodic nanostructures. The femtosecond laser is focused onto the material through a lens with a focal length of 100mm. A self-organized periodic nanograting is observed in the HR path when we set DMD to be blank statically (function as mirror). As is displayed in Fig. 7b, the periodicity of this grating is measured to be 836nm, which corresponds well with the one reported in literature [13].

Now that we have demonstrated the periodic nanostructures in high-resolution path, we employ DP-SCM system to observe its generation process. To compress the production process of self-organized periodic nanostructures into one single shot, we have conducted numerous experiments to testify the appropriate experimental conditions for observation since the repetition rate and laser power will greatly affect its nanograting generation speed. The best repetition rate and laser power in our experiment is 5kHz and 5mw respectively. Fig. 8 is the experimental results when the compressed ratio is 10, corresponding to a frame rate of 500fps when the compressed measurement is taken with an exposure time of 20ms. We see from Fig. 8b that the nanograting is growing at a slow pace. In the reconstruction frames, the initial half of the frames almost entirely capture this growth, while the subsequent time stamps show no discernible change in the nanograting's growth. This is attributed to the insufficient speed of the imaging process. To visualize the whole growing process, we increase the compressed ratio to 20, corresponding to a high-speed camera with a frame rate of 1000 fps when the exposure time for one measurement is set to 20ms. As shown in Fig. 9, it is evident that the periodic structure can be visualized within 20 frames. These two reconstructed videos are placed in Visualizations 4 (CR=10) and Visualizations 5 (CR=20). The 1st reconstructed frame shows no periodic structure while a obvious growing can be seen in the following reconstructed frames, such as frame 11 and frame 19. We want to emphasize that many laser pulses are involved in a single frame. To explore nanograting growth with fewer laser pulse, we reduced the femtosecond laser's repetition rate to 1 kHz, aligning it with the twice the speed of reconstructed frame rate. In this way, each reconstructed frame captures the interaction of two laser pulses with the sample. The results are presented in Supplement Material Fig. S3.

Notice that the signal-to-noise-ratio of the reconstructed frames in compressed ratio of 20 is much lower compared with the one in compressed ratio of 10. This is due to the fact that higher compressed ratio always comes with lower dynamic range since shorter temporal exposure (temporal resolution) is present. More details of this aspect can be found in Supplement Material Fig. S4. This problem can be mitigated by devising novel algorithms working at low light conditions or using low-light images to train the network.

Conclusion

In summary, in-process real-time monitoring of the laser material manufacturing is demonstrated by using our custom-built DP-SCM system. To evaluate the performance of the DP-SCM system, the FOV, the lateral resolution is measured to be 2mm and 775nm respectively. A frame rate of 500fps is validated by using a conventional camera working at a frame rate of 50fps. Moreover, we compare three reconstruction algorithms and choose the state-of-the-art EfficientSCI algorithm. To validate the system's feasibility in in-process laser material processing,

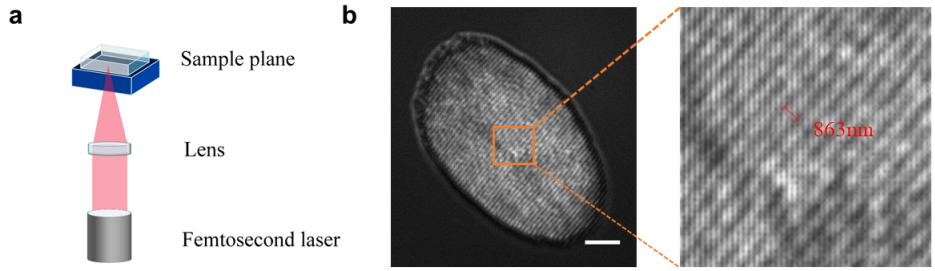

Fig. 7. Self-organized periodic nanostructures. **a** Setup for generating self-organized periodic nanostructures. **b** Captured nanograting structure in high-resolution path (left), with zoom-in image (right). Scale bar in **b** is 10um.

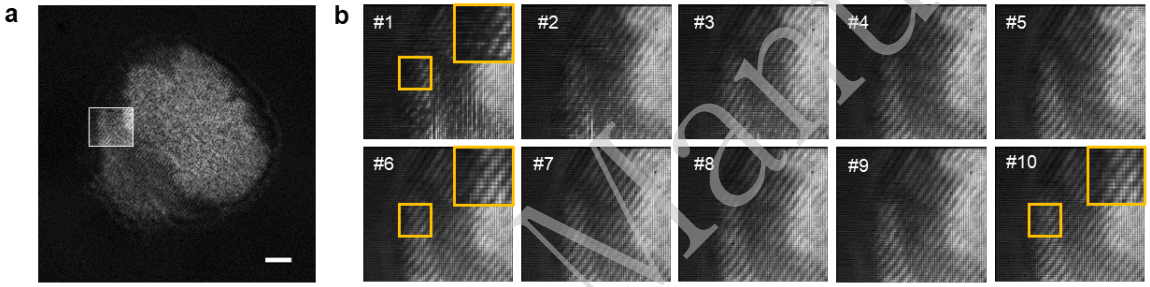

Fig. 8. *In-situ* and real-time monitoring of the growth of self-organized periodic nanostructures with a compressed ratio of 10. **a** Compressed measurement captured under 20ms in high-resolution path. **b** Reconstructed frames (corresponding to the white box area in **a**) with magnified images on the up-right corner (corresponding to the yellow box area). Scale bar in **a** is 10um.

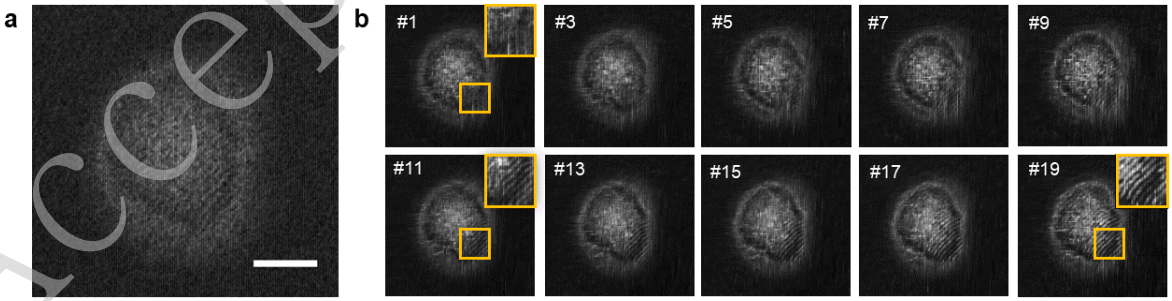

Fig. 9. *In-situ* and real-time monitoring of the growth of self-organized periodic nanostructures with a compressed ratio of 20. **a** Compressed measurement captured under 20ms in high-resolution path. **b** Reconstructed frames are presented, showcasing one frame for every two images, along with magnified images in the upper-right corner, corresponding to the yellow box area. Scale bar in **a** is 10um.

we conduct experiments when the laser or translation stage is scanning across the sample plane. The results showcase DP-SCM's superiority in imaging speed in terms of laser material processing. Furthermore, we perform *in-situ* and real-time monitoring of the growth of the self-organized periodic nanostructures. With an imaging speed at a frame rate 500fps (exposure time of single measurement=20ms, CR=10), we are able to witness the partial growth of nanograting. When increasing the CR to 20, corresponding to an imaging speed of 1000fps, the whole growing process of nanograting can be visually observed. Therefore, we validate DP-SCM is capable of visualizing the ultrafast laser processing and uncovering novel phenomenons of laser-material interaction. Note that the imaging setup is in a transmissive module, which can also be adapted into refection setup according to the transparency of manufacturing sample.

Our proposed method features wide-field and high-resolution imaging at high-speed imaging. Wide-field and high-resolution imaging help visualize the whole processing with finer details, which is applicable to all imaging systems that requires in-situ monitoring. For scenarios that requires higher imaging speed, conventional cameras (working at a frame rate below 500fps) fail to provide enough temporally resolved information, our method offers a fast imaging way to visualize the process with relatively low cost and low bandwidth.

The snapshot compressive imaging not only compresses the temporal signals but also 3D [47] and spectral information [48], which can also be used to inspect the 3D structure [49] and structure color [50] in *in-situ* real-time laser processing. Lastly, this system can be readily accommodated into other laser processing setup to enable high-speed imaging. We expect that this snapshot compressive imaging system can find more applications in fields of laser processing and other manufacturing inspection.

Acknowledgement

This work was supported by National Natural Science Foundation of China (62271414), Science Fund for Distinguished Young Scholars of Zhejiang Province (LR23F010001), Research Center for Industries of the Future (RCIF) at Westlake University and and the Key Project of Westlake Institute for Optoelectronics (Grant No. 2023GD007).

Author contributions

X.Y. and L.S. contributed the original idea to adopt DP-SCM as a real-time monitoring tool for laser material processing and supervised this study. X.W. built the setup, performed experiments and wrote the original manuscript. M.C. reconstructed the data and wrote the manuscript. Z.C., T.L. and Y.D. assisted in data acquisition. Z.C. and X.L. polished the idea. J.G. provided the processing material and assisted in constructing the experimental setup.

Conflict of interest

The authors declare no conflicts of interest.

References

[1] Zhu, X. et al. Plasmonic colour laser printing. *Nat Nanotechnol* **11**, 325–9 (2016).

[2] Kerse, C. et al. Ablation-cooled material removal with ultrafast bursts of pulses. *Nature* **537**, 84–88 (2016).

[3] Jeon, H. et al. Directing cell migration and organization via nanocrater-patterned cell-repellent interfaces. *Nat Mater* **14**, 918–23 (2015).

[4] Sun, K. et al. Three-dimensional direct lithography of stable perovskite nanocrystals in glass. *Science* **375**, 307–310 (2022).

[5] Tan, D., Zhang, B. & Qiu, J. Ultrafast laser direct writing in glass: Thermal accumulation engineering and applications. *Laser & Photonics Reviews* **15**, 2000455 (2021).

[6] Wang, J. et al. Laser machining fundamentals: micro, nano, atomic and close-to-atomic scales. *International Journal of Extreme Manufacturing* **5**, 012005 (2023).

[7] Malinauskas, M. et al. Ultrafast laser processing of materials: from science to industry. *Light: Science & Applications* **5**, e16133–e16133 (2016).

[8] Okamoto, Y. et al. High-quality micro-shape fabrication of monocrystalline diamond by nanosecond pulsed laser and acid cleaning. *International Journal of Extreme Manufacturing* **4**, 025301 (2022).

[9] Wokosin, D. L. et al. All-solid-state ultrafast lasers facilitate multiphoton excitation fluorescence imaging. *IEEE Journal of Selected Topics in Quantum Electronics* **2**, 1051–1065 (1996).

[10] Davis, K. M. et al. Writing waveguides in glass with a femtosecond laser. *Opt Lett* **21**, 1729–31 (1996).

[11] Zhang, Y. et al. Femtosecond laser direct writing of functional stimulus-responsive structures and applications. *International Journal of Extreme Manufacturing* **5**, 042012 (2023).

[12] Zhang, D., Liu, R. & Li, Z. Irregular lipss produced on metals by single linearly polarized femtosecond laser. *International Journal of Extreme Manufacturing* **4**, 015102 (2021).

[13] Geng, J. et al. Quasicylindrical waves for ordered nanostructuring. *Nano Letters* **22**, 9658–9663 (2022).

[14] Geng, J. et al. Surface plasmons interference nanogratings: wafer-scale laser direct structuring in seconds. *Light: Science & Applications* **11**, 189 (2022).

[15] Kawabata, S. et al. Two-dimensional laser-induced periodic surface structures formed on crystalline silicon by ghz burst mode femtosecond laser pulses. *International Journal of Extreme Manufacturing* **5**, 015004 (2023).

[16] Saha, S. K. et al. Radiopaque resists for two-photon lithography to enable submicron 3d imaging of polymer parts via x-ray computed tomography. *ACS Appl Mater Interfaces* **10**, 1164–1172 (2018).

[17] Mayer, F. et al. 3d fluorescence-based security features by 3d laser lithography. *Advanced Materials Technologies* **2**, 1700212 (2017).

[18] Hahn, V. et al. Two-step absorption instead of two-photon absorption in 3d nanoprinting. *Nature Photonics* **15**, 932–938 (2021).

[19] Lamont, A. C. et al. Direct laser writing of a titanium dioxide-laden retinal cone phantom for adaptive optics-optical coherence tomography. *Optical Materials Express* **10**, 2757–2767 (2020).

[20] Lee, X. Y. et al. Automated detection of part quality during two-photon lithography via deep learning. *Additive Manufacturing* **36**, 101444 (2020).

[21] Hasegawa, S. et al. In-process monitoring in laser grooving with line-shaped femtosecond pulses using optical coherence tomography. *Light: Advanced Manufacturing* **3**, 1 (2022).

[22] Zvagelsky, R. et al. Towards in-situ diagnostics of multi-photon 3d laser printing using optical coherence tomography. *Light: Advanced Manufacturing* **3**, 1 (2022).

[23] Baldacchini, T. & Zadoyan, R. In situ and real time monitoring of two-photon polymerization using broadband coherent anti-stokes raman scattering microscopy. *Optics Express* **18**, 19219–19231 (2010).

[24] Zong, W. et al. Miniature two-photon microscopy for enlarged field-of-view, multi-plane and long-term brain imaging. *Nature Methods* **18**, 46–49 (2021).

[25] Yao, J. et al. Exploiting the potential of commercial objectives to extend the field of view of two-photon microscopy by adaptive optics. *Optics Letters* **47**, 989–992 (2022).

[26] Zheng, G., Horstmeyer, R. & Yang, C. Wide-field, high-resolution fourier ptychographic microscopy. *Nature Photonics* **7**, 739–745 (2013).

[27] Zheng, G. et al. Concept, implementations and applications of fourier ptychography. *Nature Reviews Physics* **3**, 207–223 (2021).

[28] Yuan, X., Brady, D. J. & Katsaggelos, A. K. Snapshot compressive imaging: Theory, algorithms, and applications. *IEEE Signal Processing Magazine* **38**, 65–88 (2021).

[29] Dou, Y. et al. Coded aperture temporal compressive digital holographic microscopy. *Optics Letters* **48**, 5427–5430 (2023).

[30] Wang, P. et al. Full-resolution and full-dynamic-range coded aperture compressive temporal imaging. *Optics Letters* **48**, 4813–4816 (2023).

[31] Chen, Z. et al. Physics-driven deep learning enables temporal compressive coherent diffraction imaging. *Optica* **9**, 677–680 (2022).

[32] Wang, L. et al. Spatial-temporal transformer for video snapshot compressive imaging. *IEEE Transactions on Pattern Analysis and Machine Intelligence* **45**, 9072–9089 (2023).

[33] Meng, Z., Yuan, X. & Jalali, S. Deep unfolding for snapshot compressive imaging. *International Journal of Computer Vision* **131**, 2933–2958 (2023).

[34] Wang, L., Cao, M. & Yuan, X. Efficientsci: Densely connected network with space-time factorization for large-scale video snapshot compressive imaging. In IEEE/CVF Conference on Computer Vision and Pattern Recognition (CVPR), 18477–18486 (2023). http://dx.doi.org/10.1109/CVPR52729.2023.01772.

[35] Yuan, X. et al. Plug-and-play algorithms for video snapshot compressive imaging. *IEEE Transactions on Pattern Analysis and Machine Intelligence* **44**, 7093–7111 (2022).

[36] Yuan, X. Generalized alternating projection based total variation minimization for compressive sensing. In IEEE International Conference on Image Processing (ICIP), 2539–2543 (2016). http://dx.doi.org/10.1109/ICIP.2016.7532817.

[37] Qiao, M. et al. Deep learning for video compressive sensing. *APL Photonics* **5** (2020).

[38] Cheng, Z. et al. Recurrent neural networks for snapshot compressive imaging. *IEEE Transactions on Pattern Analysis and Machine Intelligence* **45**, 2264–2281 (2023).

[39] Gao, L. et al. Single-shot compressed ultrafast photography at one hundred billion frames per second. *Nature* **516**, 74–77 (2014).

[40] Liu, X. et al. Single-shot compressed optical-streaking ultra-high-speed photography. *Optics letters* **44**, 1387–1390 (2019).

[41] Wang, P., Liang, J. & Wang, L. V. Single-shot ultrafast imaging attaining 70 trillion frames per second. *Nature communications* **11**, 2091 (2020).

[42] Zhu, L. et al. Space-and intensity-constrained reconstruction for compressed ultrafast photography. *Optica* **3**, 694–697 (2016).

[43] Lai, Y. et al. Single-shot ultraviolet compressed ultrafast photography. *Laser & Photonics Reviews* **14**, 2000122 (2020).

[44] Ma, Y., Feng, X. & Gao, L. Deep-learning-based image reconstruction for compressed ultrafast photography. *Opt. Lett.* **45**, 4400–4403 (Aug 2020).

[45] Lu, Y. et al. Compressed ultrafast spectral-temporal photography. *Phys. Rev. Lett.* **122**, 193904 (May 2019).

[46] Kingma, D. & Ba, J. Adam: A method for stochastic optimization. *International Conference on Learning Representations* (12 2014).

[47] Qiao, M. et al. Snapshot coherence tomographic imaging. *IEEE Transactions on Computational Imaging* **7**, 624–637 (2021).

[48] Wang, L. et al. Snapshot spectral compressive imaging reconstruction using convolution and contextual transformer. *Photonics Research* **10**, 1848–1858 (2022).

[49] Wang, X., Yuan, X. & Shi, L. Optical coherence tomography—in situ and high-speed 3d imaging for laser materials processing. *Light: Science & Applications* **11**, 280 (2022).

[50] Geng, J. et al. High-speed laser writing of structural colors for full-color inkless printing. *Nature Communications* **14**, 565 (2023).